https://doi.org/10.5194/egusphere-2025-6130
Preprint. Discussion started: 27 December 2025

On the capability of the Changing Atmosphere Infra-Red Tomography explorer (CAIRT) candidate mission to constrain O_3 and H_2O in the upper troposphere and lower stratosphere

Quentin Errera[1], Marc Op de beeck[1], Stefan Bender[2], Johannes Flemming[3], Bernd Funke[2], Alex Hoffmann[4], Michael Höpfner[5], Nathaniel Livesey[6], Gabriele Poli[7], Didier Pieroux[1], Piera Raspollini[7], and Björn-Martin Sinnhuber[5]

[1]Royal Belgian Institute for Space Aeronomy (BIRA-IASB), Brussels, Belgium
[2]Instituto de Astrofísica de Andalucía (CSIC), Granada, Spain
[3]Research Department, European Centre for Medium-Range Weather Forecasts, Reading, UK
[4]European Space Research and Technology Centre, European Space Agency (ESA/ESTEC), Noordwijk, The Netherlands
[5]Institute of Meteorology and Climate Research - Atmospheric Trace Gases and Remote Sensing (IMKASF), Karlsruhe Institute of Technology (KIT), Karlsruhe, Germany
[6]Jet Propulsion Laboratory, California Institute of Technology, Pasadena, California, USA
[7]Instituto di Fisica Applicata "N. Carrara" (IFAC) del Consiglio Nazionale delle Ricerche (CNR), Firenze, Italy

Correspondence: Quentin Errera (quentin.errera@aeronomie.be)

Abstract. The Changing Atmosphere Infra-Red Tomography Explorer (CAIRT) is a satellite mission concept that was proposed within ESA's Earth Explorer 11 (EE11) programme. Although it was not selected for implementation in the EE11 competition, the CAIRT concept was assessed as scientifically and technically mature and could be implemented under another ESA framework or through international collaboration. The mission is conceived to achieve a step change in our understanding of the coupling between atmospheric circulation, composition, and regional climate. The CAIRT concept is based on limb infrared tomography of the atmosphere from the troposphere to the lower thermosphere (between ∼5 and ∼115 km altitude) with a ∼400 km-wide swath, providing a three-dimensional view of atmospheric structure at unprecedented scales.

This paper investigates the capability of CAIRT to resolve vertical gradients of ozone (O_3) and water vapour (H_2O) in the upper troposphere and lower stratosphere (UTLS) using an Observing System Simulation Experiment (OSSE). In this experiment, a reference atmosphere – the nature run in OSSE terminology – is built from the Copernicus Atmosphere Monitoring Service (CAMS) control simulation between October 2021 and March 2022. The nature run is used to synthesise CAIRT observations of O_3 and H_2O, employing a CAIRT orbit simulator and a simulator that accounts for CAIRT's expected measurement errors, vertical and along-track vertical resolution. Simulated CAIRT observations are then assimilated with the Belgian Assimilation System for Chemical ObsErvations (BASCOE) to produce analyses of O_3 and H_2O (the assimilation run). To quantify the added value of CAIRT data, a BASCOE control run without CAIRT assimilation is also performed. For comparison, simulated Aura Microwave Limb Sounder (MLS) O_3 and H_2O observations are also assimilated, allowing the performance of CAIRT to be evaluated relative to this reference instrument.

The results show that CAIRT (1) O_3 observations are able to constrain BASCOE analyses down to 7 km altitude – several kilometres lower (and thus better) than MLS – and (2) H_2O observations can constrain BASCOE down to the tropopause

https://doi.org/10.5194/egusphere-2025-6130
Preprint. Discussion started: 27 December 2025

region, with slightly better performance than MLS at high latitudes. Additional sensitivity tests assess the impact of CAIRT systematic errors, cloud coverage, and reduced swath width.

1 Introduction

The upper troposphere lower stratosphere (UTLS) region plays a critical role in regulating the Earth's climate. Ozone (O_3) and water vapour (H_2O), which are among the most effective greenhouse gases, exert their largest radiative effects in the upper troposphere and around the tropopause (Lacis et al., 1990; Riese et al., 2012). Changes in the UTLS composition therefore have a direct impact on surface temperature (Solomon et al., 2010; Riese et al., 2012). One of the key processes shaping the distribution of these gases is the Brewer-Dobson circulation (BDC) – the large-scale circulation system that spans the middle atmosphere between roughly 10 and 80 km altitude. Climate models consistently predict that the BDC will accelerate in response to global climate change (Li et al., 2012; Butchart, 2014), with significant implications for the distribution of trace gases in the UTLS (McLandress and Shepherd, 2009; Hegglin and Shepherd, 2009). This includes increased exchange across the tropopause, potentially injecting O_3-rich stratospheric air into the upper troposphere (Hsu and Prather, 2009; Abalos et al., 2020).

To better understand these processes, amongst others, the Changing Atmosphere Infra-Red Tomography Explorer (CAIRT) was proposed to the European Space Agency (ESA) as a candidate for Earth Explorer 11 (EE11), the ESA's Earth observation flagship missions. CAIRT was down-selected for Phase 0 pre-definition studies between 2021 and 2023 and then subject to Phase A feasibility studies until mid-2025. Although CAIRT was not selected for implementation in the EE11 competition, the mission concept was assessed as scientifically and technically mature, and could still be implemented under another ESA programme or through international collaboration.

CAIRT is designed to employ a limb-imaging Fourier Transform Spectrometer (FTS) to observe the atmosphere from 5 to 115 km of altitude in the thermal infrared spectral domain, providing observations of temperature, O_3, and H_2O, among numerous other trace gases, with unprecedented spatial resolution relying on a tomographic retrieval approach. If implemented, CAIRT would improve our understanding of how changes in the BDC influence the distribution of O_3 and H_2O in the UTLS by observing small-scale structures and gradients of these gases across the tropopause.

Moreover, CAIRT UTLS H_2O data would be highly relevant for numerical weather prediction (NWP) systems. Many NWP models exhibit a cold temperature bias in the tropopause region caused by longwave radiative cooling associated with a moist bias in this region (Bland et al., 2021). The origin of this moist bias has been linked to excessive numerical diffusion in model transport schemes around the tropopause (Charlesworth et al., 2023). Recent updates to the European Centre for Medium-Range Weather Forecasts (ECMWF) Integrated Forecast System (IFS) have reintroduced water vapour data assimilation profiles – particularly those from the Microwave Limb Sounder (MLS) – showing significant improvement in temperature forecasts (Semane and Bonavita, 2025).

The present study has two goals. First, it aims to assess whether CAIRT measurement requirements are adequate to support the CAIRT scientific objectives targeting UTLS ozone and water vapour, with emphasis on providing scientific and societal

https://doi.org/10.5194/egusphere-2025-6130
Preprint. Discussion started: 27 December 2025

added value via improved constraints on these radiative forcing gases. Second, it aims to compare CAIRT's capabilities with those of the existing MLS instrument, which serves as one of the main references for O_3 and H_2O observations in the UTLS (SPARC, 2017). This assessment is performed using an Observing System Simulation Experiment (OSSE).

OSSEs are typically designed to investigate the potential impacts of prospective observing systems using data assimilation (DA) techniques (Masutani et al., 2010; Timmermans et al., 2015; Errera et al., 2021). They are set up using several numerical experiments: the nature run (NR), the control run (CR), and at least one assimilation run (AR). The nature run corresponds to a model simulation defining the true state of the atmosphere. It is used to simulate observations with the instrument of interest and, if needed, with other existing observing systems used in data assimilation. The control run, being either a free model run or a data assimilation run using only simulated observations of existing instruments, provides the baseline atmospheric state and serves to evaluate the impact of the new instrument. The assimilation run includes the new observations in addition to those assimilated in the CR, if any. The comparison between AR-NR and CR-NR differences quantifies the added value of the new instrument. Additional assimilation runs can also be included to test alternative instrument configurations. To avoid the identical-twin problem, which can lead to over-optimistic results, assimilation and control runs should employ a different model than the nature run. This ensures that improvements in the AR relative to the CR are primarily due to the assimilation of new observations. Although OSSEs have traditionally been used to evaluate meteorological satellite systems, several studies have also applied this technique to instruments measuring atmospheric composition (Claeyman et al., 2011; Timmermans et al., 2015; Abida et al., 2017; Errera et al., 2021).

This paper is organized as follows. The concept of CAIRT and its capabilities to observe the UTLS composition are briefly introduced in Sect. 2. The nature run is presented in Sect. 3. The simulated observations of CAIRT and MLS are described in Sects. 4 and 5, respectively, followed by a discussion comparing the performance of both instruments in Sect. 6. The control and assimilation runs are presented in Sect. 7. Results are provided in Sect. 8, followed by the conclusions.

2 The CAIRT Candidate Mission

This section provides a concise overview of the CAIRT mission concept; further details are available in Sinnhuber et al. (in reveiw) and in the CAIRT Report for Mission Selection (ESA, 2025a). CAIRT aims to observe temperature and trace gases from infrared emission spectra of the Earth's atmosphere measured from a satellite in limb-viewing geometry. The instrument concept is based on infrared imaging, allowing for simultaneous vertical coverage (approximately 5-115 km altitude) and horizontal across-track coverage (a swath width of about 300-500 km, depending on design trade-offs). Each pixel of the imaging detector provides an interferogram within a finite acquisition time, which can be processed into a line-of-sight limb emission radiance spectrum (Level-1 data).

By acquiring new interferograms every ∼7.5 s, arrays of limb line-of-sight spectral radiance measurements would be acquired approximately every 50 km along the satellite track, enabling tomographic retrieval. Data from several pixels are typically binned to achieve sampling of about 1 km in the vertical and finer than 50 km in the across-track direction around the tangent point. Furthermore, to facilitate potential synergies with nadir instruments, CAIRT tangent points are designed to be

https://doi.org/10.5194/egusphere-2025-6130
Preprint. Discussion started: 27 December 2025

Table 1. CAIRT Level-2 requirements for O_3 and H_2O in the upper troposphere (UT) and lower stratosphere (LS). Values are given as Goals (Thresholds).

Product	Region	Uncertainty	Vertic. resolution (km)	Horiz. ACT resolution (km)
O_3	UT	15 (30) ppbv	1 (2)	100 (200)
	LS	50 (150) ppbv	1 (2)	100 (200)
H_2O	UT	5 (10) %	1 (2)	100 (200)
	LS	5 (10) %	1 (3)	100 (200)

co-registered with MetOp second generation (SG) nadir instruments, particularly with the Infrared Atmospheric Sounding Interferometer New Generation (IASI-NG), allowing both satellites to sample approximately the same air masses simultaneously.

The CAIRT spectral range is specified in the long- to mid-wave infrared regions (718-2200 cm^{-1}) with a spectral resolution better than 0.25 cm^{-1}, enabling the retrieval of temperature and numerous trace gases (O_3, H_2O, CH_4, nitrogen and sulfur species, CFCs, SF_6, and others). In the UTLS, CAIRT O_3 observational requirements are specified with a vertical resolution better than 2 km, a horizontal (across-track, ACT) resolution better than 100 km, and a total uncertainty better than 30 ppbv in the upper troposphere and better than 150 ppbv between the lower stratosphere and 30 km altitude (see Table 1). For H_2O, the specified spatial resolution is similar, with a total uncertainty better than 10 %. These requirements are designed to ensure sensitivity to stratosphere–troposphere exchange processes, such as stratospheric intrusions.

The Level-1 limb radiance spectra corresponding to multiple across-track spatial samples are averaged to reduce noise before Level-2 retrievals (see Sects. 4.4 and 4.5).

CAIRT builds upon the strong space heritage of infrared limb emission measurements established by the Michelson Interferometer for Passive Atmospheric Sounding (MIPAS) instrument onboard Envisat, which operated between 2002 and 2012 (Fischer et al., 2008). MIPAS was an FTS scanning instrument with a single pixel detector, providing one retrieved profile approximately every 400 km – over an order of magnitude fewer profiles than CAIRT. CAIRT would deliver roughly 12 times more profiles than MLS, which provides one profile every 167 km along the orbit track (see Sect. 5). If implemented, CAIRT would be the first infrared limb imager in space, building on the heritage of the Gimballed Limb Observer for Radiance Imaging of the Atmosphere (GLORIA), which has flown on balloons and aircraft since 2011 (Riese et al., 2014; Friedl-Vallon et al., 2014). Experience with the airborne demonstrator instrument GLORIA provides confidence that the estimated performance of the CAIRT concept are realistic.

https://doi.org/10.5194/egusphere-2025-6130
Preprint. Discussion started: 27 December 2025

3 The nature run

In this study, a CAMS control simulation is used as the nature run providing the synthetic truth state for ozone, water vapour and cloud. It is based on the Integrated Forecast System for COMPOsition (IFS-COMPO) cycle 47r3. The meteorological upgrade implemented in cycle 47r3 is described in Forbes et al. (2021), while the chemical scheme is summarized in Arola et al. (2022) and references therein. This cycle became operational in October 2021 but had been running as an experimental control simulation since March of that year.

Unlike the operational CAMS analyses, the control simulation does not assimilate either chemical or meteorological observations. However, its meteorology – including the specific humidity – is reinitialized every 24 hours from the operational CAMS analyses at 00 UTC. The simulation employs a reduced Gaussian grid at TL511 horizontal resolution (approximately 40 km) with 137 vertical levels, providing a vertical resolution of about 400 m at 50 hPa, 300 m in the UTLS, and getting finer toward the surface.

In IFS-COMPO 47r3, ozone is represented using a detailed chemistry scheme in the troposphere and a linearized parameterization in the stratosphere (Flemming et al., 2015). For water vapour, we use the specific humidity field provided by IFS-COMPO. The control simulation was selected because its output is archived every 3 hours, compared to every 6 hours for the operational analyses. In this configuration, ozone is not constrained by any observations, whereas water vapour is indirectly constrained through the daily reinitialization of specific humidity from the CAMS analyses, within with this variable is assimilated in the troposphere.

Ozone from the CAMS control simulation is routinely evaluated against a wide range of observational datasets by the CAMS Evaluation and Quality Control (EQC) service (see, e.g., Arola et al., 2022, and https://atmosphere.copernicus.eu/eqa-reports-global-services, last access Nov. 13, 2025). Following the CAMS EQC methodology, ozone from the CAMS control simulation was compared with ozonesonde and a set of limb-sounding profiles for the period October-December 2021 (see Fig. S1). The rationale for selecting this period is provided in the following paragraphs.

In the stratosphere (above 100 hPa), except over the southern polar region, the agreement between the CAMS control simulation and both ozonesonde and satellite observations is generally good. The mean bias remains within ± 10 %, the standard deviation of the difference is below 10 %, and the correlation typically exceeds 0.8. In the troposphere, the agreement is worse: comparisons with ozonesondes reveal positive biases of +10 % to +20 % in the tropics and biases within ± 10 % at mid-latitudes. The standard deviation increases notably in the tropics, although the correlation remains between 0.5 and 0.8. While ozone from the operational CAMS analysis exhibits better agreement due to the assimilation of multiple satellite ozone retrievals, the quality of the control simulation is considered sufficient for the purposes of this study.

For specific humidity, major upgrades to the moist-physics parameterizations and the assimilation of satellite observations were introduced in IFS-COMPO cycle 47r3 (Forbes et al., 2021), reducing the stratospheric temperature bias by up to 50 %. Using the same evaluation methodology as for ozone, specific humidity from the CAMS control simulation was compared with measurements from two limb-sounding instruments (see Fig. S2). Because the stratospheric water vapour content increased by

https://doi.org/10.5194/egusphere-2025-6130
Preprint. Discussion started: 27 December 2025

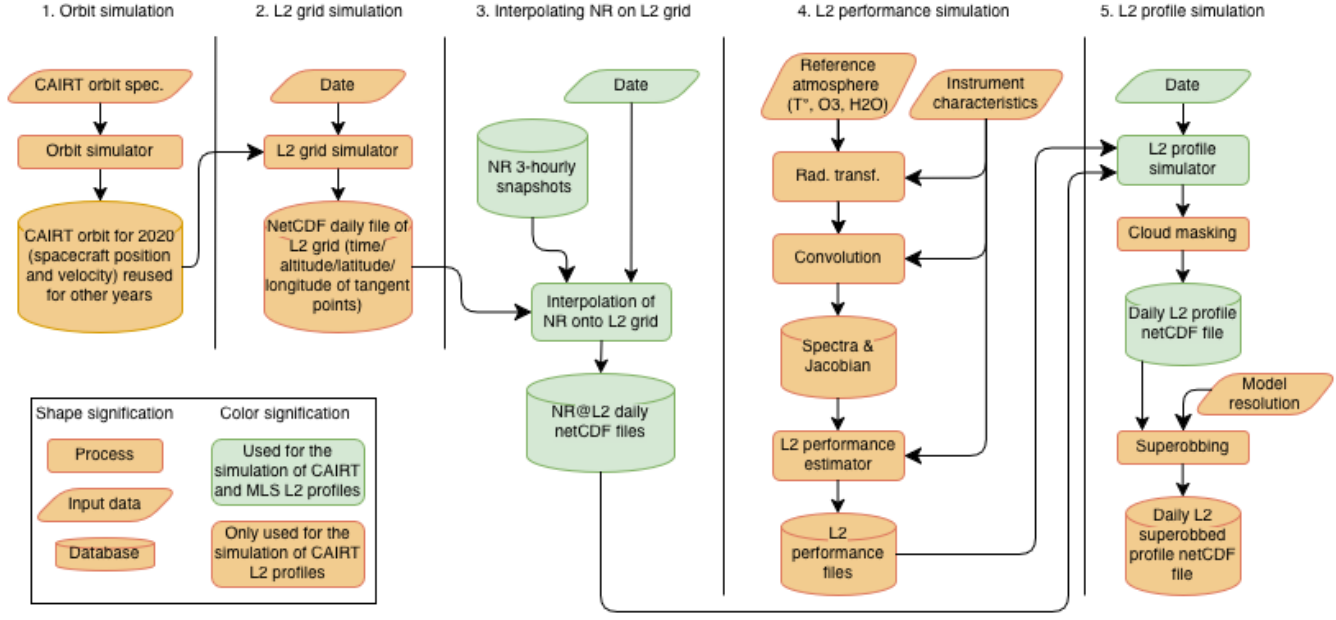

Figure 1. Processing chain used to simulate CAIRT and MLS Level-2 profiles. Processes in orange are only done for CAIRT while processes in green are done for CAIRT and MLS.

approximately 10 % following the Hunga eruption in mid-January 2022 (Millán et al., 2022), and since this source of water vapour is not represented in CAMS, the comparison was restricted to the October-December 2021 period.

In the stratosphere (above 100 hPa), the mean bias in specific humidity is positive, between 0 % and 10 %, with a standard deviation below 10 %. In the troposphere, both the mean bias and standard deviation increase with pressure, reaching approximately +30 % and +50 %, respectively, at 250 hPa. The correlation remains relatively high above 50 hPa and below 200 hPa, but decreases to around 0.5 between these pressure levels, except in the tropics near 50 hPa where it approaches zero. Nevertheless, as for ozone, the quality of the control simulation is deemed adequate for use in this study.

The control simulation is archived in the ECMWF MARS system, and the corresponding MARS parameters required for data retrieval are provided in the Data Availability section at the end of this paper.

4 Simulating CAIRT observations

Simulating CAIRT Level-2 (L2) profiles from the nature run involves several steps, illustrated in Fig. 1. First, the satellite orbit must be simulated, i.e. the satellite position and velocity vectors are determined at a frequency consistent with the along-track sampling. Second, given the satellite position and velocity and the CAIRT viewing direction, the CAIRT retrieval grid is computed, providing the geolocation of the points observed by CAIRT. Third, the nature run is interpolated at the observed points, yielding the NR@L2 dataset.

https://doi.org/10.5194/egusphere-2025-6130
Preprint. Discussion started: 27 December 2025

The performance characteristics of the L2 products, namely the averaging kernels and observational uncertainties, must also be simulated (step 4). Subsequently (step 5), the simulated L2 profiles are generated by convolving NR@L2 with the L2 performance characteristics. To account for the potential saturation of Level-1 (L1) spectra caused by the presence of clouds, cloud information is incorporated at this stage.

Because the number of CAIRT profiles is significantly larger than that of any existing limb-sounding instrument, direct assimilation into the BASCOE-EnKF system would lead to memory overflow. This is a well-known issue in data assimilation (DA), for which a common solution is the generation of superobservations (often referred to as superobbing in DA terminology), obtained by combining observations available at the same time within the same model grid cell.

All these steps are described in detail in the following subsections.

4.1 CAIRT orbit simulation

As mentioned in Sect. 2, one of the CAIRT requirements is to provide observations co-registrated with IASI-NG onboard MetopSG. The simulation of the CAIRT orbit (step 1 in Fig. 1) was thus performed using the MetOp-SG orbit specifications as a reference, with adjustments to the longitude of the ascending node to ensure that the MetOp-SG Nadir instruments and CAIRT sample the same air masses simultaneously (see Table S1). ESA's Earth Observation Mission Software was employed for the simulation (ESA, 2025a, b).

An Orbit Scenario File was first generated (ESA, 2024, 2025c) to define the CAIRT orbit, which was subsequently used to compute the satellite position and velocity vectors with a propagation step of 7.56 s, corresponding to an along-track sampling step of approximately 50 km. The results of the orbit simulation were stored in an ASCII file (available on the CAIRT Zenodo repository, see Code and Data Availability section below) containing: the epoch of each propagation step (UTC), satellite position and velocity vectors in the Earth-Fixed Earth-Centered (EFEC) reference frame, latitude and longitude of the sub-satellite point, and the satellite's geodetic height.

4.2 CAIRT L2 geolocation simulation

Providing the orbit parameters, the second step is to set up the CAIRT L2 grids, i.e. the time and position where CAIRT L2 profiles will be available (step 2 in Fig. 1). This step is subdivided into two tasks. The first one is to estimate the geodetic tangent point (TP) at 30 km of altitude from a limb-viewing instrument looking backward on a polar orbit like CAIRT. An initial estimate is obtained from a spherical-Earth approximation, which provides a simple analytic relationship between spacecraft altitude, viewing geometry, and desired TP altitude. This initial value slightly overestimates the TP altitude when Earth's oblateness is considered, and it is therefore refined iteratively until the resulting TP altitude matches the requested value within a tolerance of 1 meter.

CAIRT being an imager, several profiles on parallel tracks will be retrieved at the same time and the second task is to find the geolocation of these profiles. For O_3 and H_2O in the UTLS, the ACT sampling has been set to 100 km (see Sect. 2, while for temperature, the goal and threshold are, respectively, 25 and 50 km ACT). With a swath of 400 km, this will provide four profiles per image. Their geolocations are computed left and right to the TP at 30 km and in a perpendicular plane to the LoS.

https://doi.org/10.5194/egusphere-2025-6130
Preprint. Discussion started: 27 December 2025

4.3 Interpolation of the nature run on the L2 grid

The regridding of NR onto the CAIRT L2 grid (step 3 in Fig. 1) is performed using a subset of the BASCOE system, namely its BASCOE-MAO mode (Model At Observation). As a data assimilation system, BASCOE includes routines to read model fields and observation files, as well as an observation operator to interpolate model fields to the geolocations of the observations. In its MAO configuration, model fields are taken from snapshot files rather than being simulated by the BASCOE model. In this procedure, the 3-hourly CAMS snapshot fields are linearly interpolated in time and space to the geolocations of the CAIRT tangent points. This is the same procedure used in the CAMS EQC project to validate CAMS stratospheric ozone analyses and forecasts.

4.4 CAIRT L2 Performance Simulation

To simulate CAIRT L2 profiles, the L2 performance must be estimated (step 4 in Fig. 1), including the averaging kernels and uncertainties under different atmospheric conditions. This simulation should balance computational efficiency with sufficient complexity to provide a realistic representation of the observing system's (including the instrument's) performance.

A parametric approach based on linear retrieval simulations is employed, allowing efficient generation of large volumes of emulated L2 data while realistically representing the instrument performance. This approach will be presented in Funke et al. (in prep.) and is summarized below.

4.4.1 Climatology generation

A climatology of the atmospheric conditions encountered by CAIRT was created for all relevant parameters that influence spectral signatures in CAIRT's measurement range (Errera et al., in prep.). This includes O_3, H_2O, CO_2, temperature, and other trace gases. To represent variability, the climatology was computed for four representative months corresponding to different seasons (January, April, July, and October), five latitude bands (90°S–70°S, 55°S–35°S, 20°S–20°N, 35°N–55°N, and 70°N–90°N), the two overpass local times (09:30 and 21:30), and 201 vertical levels (0–200 km with 1 km spacing).

Since no single atmospheric model or dataset provides all relevant trace gases across the vertical domain between 5 and 115 km, this climatology was created by blending outputs from multiple simulations from multiple models. For ozone and water vapour in the UTLS, the climatology is based on the Whole Atmosphere Community Climate Model (WACCM, Gettelman et al., 2019) in its ACOM configuration (Atmospheric Chemistry Observations and Modeling), which has been operational since August 2019. The period considered for climatology generation was October 2019–October 2022, which was the longest available period at the time of the CAIRT Phase 0 project.

4.4.2 Radiative transfer simulations

Using the climatology and the Karlsruhe Optimized and Precise Radiative transfer Algorithm (KOPRA, Stiller, 2000), an ensemble of radiance spectra and their Jacobians was computed with 0.2 cm^{-1} spectral sampling. Perturbations were included to account for uncertainties in instrument and atmospheric parameters which are described in ESA (2025a). The resulting

https://doi.org/10.5194/egusphere-2025-6130
Preprint. Discussion started: 27 December 2025

spectra and Jacobians were then vertically and spectrally convolved with representative functions based on instrument specifications, including vertical sampling, the vertical System Energy Distribution Function (SEDF), and spectral apodization using the Norton–Beer–Strong function (Norton and Beer, 1976, 1977).

4.4.3 L2 performance estimation

For each of the different climatological conditions, L2 performance has been diagnosed based on the corresponding radiance spectra and Jacobians. Resulting output files include the two-dimensional (vertical and along-track) averaging kernels, factorized random error covariance matrices representing measurement noise, and two Monte-Carlo ensembles of systematic error profiles (corresponding to across-track correlated and uncorrelated uncertainties, respectively). This computation employs a tomographic retrieval approach for limb observations as in Steck et al. (2005). Instrument specifications based on CAIRT's threshold uncertainty assumptions - including calibration uncertainty, calibration cycle, and systematic uncertainty - were incorporated, along with error propagation from temperature and line-of-sight retrievals in the O_3 and H_2O profiles.

4.5 CAIRT L2 Profiles Simulation

CAIRT L2 profiles are simulated for a given date using the NR@L2 daily file and the L2 performance file (step 5 in Fig. 1). The simulator interpolates the L2-estimated two-dimensional (vertical and along-track) averaging kernels and errors to the time and location of each CAIRT L2 profile. The NR@L2 profiles are then convolved with the interpolated averaging kernel matrices and randomly perturbed in a manner that preserves spatial error correlations as follows:

$$\boldsymbol{y}_{l2} = \mathbf{A}\boldsymbol{y}_n + (\mathbf{I} - \mathbf{A})\boldsymbol{y}_a + \boldsymbol{\epsilon}_{rnd} + \boldsymbol{\epsilon}_{sys\_corr} + \boldsymbol{\epsilon}_{sys\_uncorr} \tag{1}$$

where $\boldsymbol{y}_{l2}$ is a simulated L2 profile, $\boldsymbol{y}_n$ is a chunk of NR@L2 profiles on the CAIRT grid spanning ± 1900 km in the along-track dimension, centered on the tangent point of $\boldsymbol{y}_{l2}$, and $\mathbf{A}$ is the CAIRT averaging kernel matrix corresponding to the geolocation of that chunk. The term $\boldsymbol{y}_a$ represents the a priori profile, and $\mathbf{I}$ is the identity matrix.

The perturbation $\boldsymbol{\epsilon}_{rnd}$ is obtained by multiplying a Gaussian random number field with the factorized random error covariance matrix. The profiles $\boldsymbol{\epsilon}_{sys\_corr}$ and $\boldsymbol{\epsilon}_{sys\_uncorr}$ represent the systematic error contributions, corresponding to the along-track correlated and uncorrelated components, respectively.

In our computation, $\boldsymbol{y}_a$ has been set to zero in order to avoid any apriori influence on the results.

The influence of clouds on the simulation of L2 profiles was also taken into account. In infrared limb sounding, spectra that are strongly affected by thick clouds are typically excluded to prevent instabilities and errors in the retrieval of trace gas concentrations. However, retrievals remain feasible in the presence of thin or small clouds. In limb-viewing geometry, the region in which trace gas information is obscured by clouds often extends beyond the actual physical cloud boundaries.

In this study, the following approach was adopted: retrievals were considered cloud-obscured when the CAMS cloud fraction exceeded 0.2. Clouds were assumed to extend vertically down to 5 km below the cloud-top altitude and horizontally over 50 km along the satellite track, thereby preventing retrievals beneath cloudy regions.

https://doi.org/10.5194/egusphere-2025-6130
Preprint. Discussion started: 27 December 2025

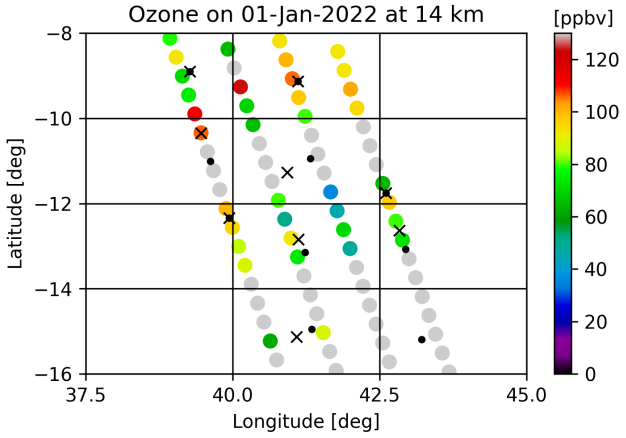

Figure 2. Coloured dots represent CAIRT L2 O_3 observations at 14 km on Jan. 1, 2022. Gray dots are CAIRT L2 observations obscured by clouds when CAMS cloud fraction is greater than 0.2. The grid represents the BASCOE spatial resolution used in the control and assimilation runs. Superobservations will be the average values of valid CAIRT L2 observations within the same BASCOE grid point, located at the black crosses. Black dots would be the locations of superobservations if no cloud filtering were used.

As previously mentioned, CAIRT will deliver substantially more profiles than existing limb instruments, e.g., approximately 12 times more than MLS. This number is too large to be handled directly by the BASCOE-EnKF system used in our OSSE. At each model time step, the system must invert a matrix whose size depends on the number of available observations multiplied by the ensemble size. With the default model time step of 30 minutes and an ensemble size of 20, this corresponds to a matrix with 6.6×10^5 points to invert (i.e., 240 measured interferograms $\times$ 4 tracks $\times$ 35 altitude levels from 5 to 40 km $\times$ 20 ensemble members). This exceeds the computational capacity of the BIRA-IASB server.

Reducing the model time step to 7.5 minutes decreases the matrix size by a factor of 4, making the computation feasible. However, this configuration produces noisy analysis increments, degrading the quality of the assimilation. This is a well-known issue in data assimilation, for which one common solution is the construction of *superobservations* (Eskes et al., 2003; Hoffman, 2018). In this approach, observations located within the same model grid cell at the same model time step are combined (see also Fig. 2).

Let N L2 observations $\boldsymbol{y}_i$ and their associated uncertainties $\boldsymbol{e}_i$ be available at the same model time step and within the same grid cell, with $i = 1 \ldots N$. The L2 superobservation $\boldsymbol{s}$ and its associated uncertainty $\boldsymbol{\sigma}$ are computed as:

$$\boldsymbol{s} = \frac{1}{N} \sum_{i=1}^{N} \boldsymbol{y}_i \tag{2}$$

$$\boldsymbol{\sigma} = \sqrt{\frac{1}{N} \sum_{i=1}^{N} \boldsymbol{e}_i^2} \tag{3}$$

https://doi.org/10.5194/egusphere-2025-6130
Preprint. Discussion started: 27 December 2025

The latitude and longitude of the superobservation are taken as the mean values of the corresponding coordinates of the individual profiles. Only CAIRT L2 observations not contaminated by clouds are included in this computation, such that the latitude and longitude of superobservations may vary with altitude.

If observation errors and correlations were perfectly represented, the use of individual observations or superobservations in data assimilation would produce identical analyses. In practice, however, superobservations reduce representativeness errors and mitigate the overweighting of dense, correlated data. As a result, the analyses typically differ slightly, often yielding smoother and more balanced fields (Duncan et al., 2024; Rijsdijk et al., 2025).

5 Simulating MLS observations

The computation of MLS simulated profiles differs from that of CAIRT profiles in that some of the required data are already available. This includes the geolocation of MLS profiles, the a priori profiles, the L2 error profiles, and the vertical averaging kernels. The MLS geolocation, a priori profiles, and L2 error profiles are obtained from MLS v5 daily observation files, while the MLS v5 vertical averaging kernels are provided for five latitudes and are independent of time and longitude.

The CAMS nature run is interpolated onto the MLS retrieval grid using BASCOE-MAO, as for CAIRT (see Sect. **??**), and is then perturbed to produce the L2 profiles $\boldsymbol{y}_{l2}$ as follows:

$$\boldsymbol{y}_{l2} = \mathbf{A}\boldsymbol{y}_n + (\mathbf{I} - \mathbf{A})\boldsymbol{y}_a + \boldsymbol{\epsilon}_p \tag{4}$$

Here, $\boldsymbol{y}_n$ represents the nature run interpolated onto the MLS grid; $\boldsymbol{y}_a$ denotes the existing MLS a priori profiles corresponding to the MLS geolocation; $\mathbf{A}$ is the MLS vertical averaging kernel matrix; and $\mathbf{I}$ is the identity matrix. Note that MLS along-track averaging kernels have not been taken into account The perturbation profile $\boldsymbol{\epsilon}_p$ is a Gaussian random profile multiplied by the MLS L2 error profile provided in the MLS data files.

Simulated profiles are only assimilated within the vertical range of validity specified in Livesey et al. (2022). This report also defines criteria for accepting or discarding profiles based on the variables "estimated precision," "quality," "convergence," and "status" provided in the MLS files. These criteria were used to flag entire profiles or portions of profiles, discarding measurements contaminated by clouds, particularly for O_3 (see discussion in the next section).

6 About Differences Between CAIRT and MLS

As previously mentioned, CAIRT will provide substantially higher sampling than MLS (or MIPAS) for O_3 and H_2O in the UTLS, delivering approximately 12 times more profiles. This is illustrated in Figs. 3 and 4e. Figure 4 compares various performance metrics for CAIRT and MLS: (a) random error, (b) systematic error, (c) vertical resolution, (d) horizontal resolution, and (e) number of available observations. For CAIRT performances discussed in Sect. 4.4, the displayed values correspond to January in the tropics and are representative of other months and latitudes. MLS performances are taken from the MLS v5 data

https://doi.org/10.5194/egusphere-2025-6130
Preprint. Discussion started: 27 December 2025

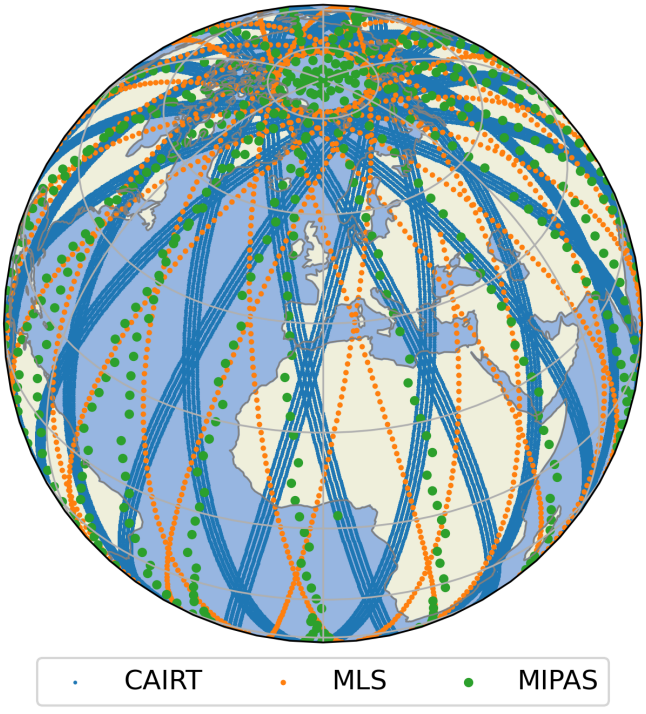

Figure 3. Illustration of CAIRT sampling for O_3 and H_2O in the UTLS compared to MLS and MIPAS. This is on Jan. 16, 2022 for CAIRT and MLS, for the same day in 2011 for MIPAS.

quality document and are generally independent of latitude and season, except for the number of observations (Livesey et al., 2022).

For O_3, CAIRT and MLS exhibit comparable random errors, whereas for H_2O, MLS shows slightly smaller (i.e., better) random errors (Fig. 4a). The systematic error profile of MLS is generally larger than that of CAIRT but remains much lower than the random error for both instruments and species (Fig. 4b). For O_3, CAIRT systematic errors exceed 50 % below 7 km in the tropics; consequently, CAIRT O_3 observations below this altitude have not been assimilated. The vertical resolutions of both instruments are comparable for O_3, while MLS generally exhibits better vertical resolution in the stratosphere for H_2O (Fig. 4c). For both species, CAIRT achieves superior horizontal resolution (Fig. 4d). The number of available observations for January is shown in Fig. 4e; the decrease with decreasing altitude is due to the presence of clouds.

Figure 5 compares CAMS ozone with the corresponding L2 simulated observations for CAIRT and MLS along an orbit on Dec. 15, 2021 (a similar figure for H_2O is provided in Fig. S3). Note that CAIRT and MLS orbits differ in time and position; therefore, this comparison provides only a qualitative indication of their differences. In the stratosphere, CAIRT and MLS observations closely match the original CAMS data, whereas in the troposphere the agreement is weaker. In the tropics, a large portion of CAIRT data below 15 km is rejected due to clouds, whereas MLS is less affected. This difference arises from the measurement techniques, as microwave observations (MLS) are less sensitive to clouds than infrared (CAIRT). Conversely,

https://doi.org/10.5194/egusphere-2025-6130
Preprint. Discussion started: 27 December 2025

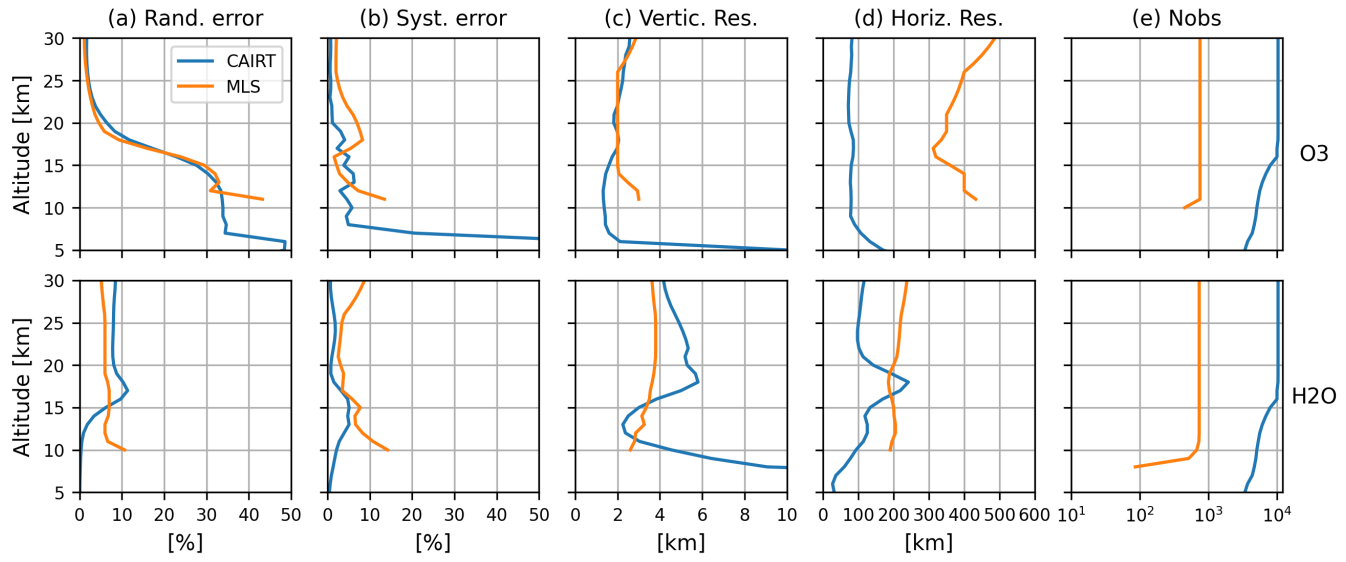

Figure 4. Performances of CAIRT (blue lines) and MLS (orange lines) for ozone (top line) and water vapour (bottom line). From left to right: random error, systematic error, vertical resolution, horizontal (along track) resolution and average number of valid observations for the period Oct. 2021-Feb. 2022. CAIRT performances are for January in the tropics. MLS performances do not depend on the latitude region or the season. While MLS data quality document provides 2-sigma systematic error, 1-sigma random and systematic error are given here for both instruments.

CAIRT provides more valid observations than MLS at mid and high latitudes. Similar patterns are observed for H_2O (see Fig. 6).

7 Control and assimilation runs

Control and assimilation experiments were conducted with the BASCOE system (Errera et al., 2021), driven by ERA5 winds and temperatures. The simulations employed a horizontal grid of 91 latitudes by 144 longitudes (approximately 250 km horizontal resolution) and 51 vertical levels, with a vertical resolution of about 1.2 km at 50 hPa, 1 km in the UTLS, and decreasing toward the surface. This configuration is considerably coarser than that of the nature run (see Sect. 3).

In the stratosphere, BASCOE, similarly to CAMS, uses a linearized ozone chemistry scheme, although the two systems are constrained by different climatological data. In the troposphere, BASCOE applies the same linearized chemical formulation as in the stratosphere, whereas CAMS employs a comprehensive tropospheric chemistry scheme (see Sect. 3).

For the experiments presented in this study, BASCOE does not account for any chemical processes involving water vapour. To prevent an unrealistic transport of tropospheric water vapour into the stratosphere, condensation is approximated by limiting the water-vapour partial pressure to the saturation vapour pressure of water ice (Murphy and Koop, 2005). Consequently, the BASCOE and CAMS configurations and simulations exhibit substantial differences in their treatment of both O_3 and H_2O.

https://doi.org/10.5194/egusphere-2025-6130
Preprint. Discussion started: 27 December 2025

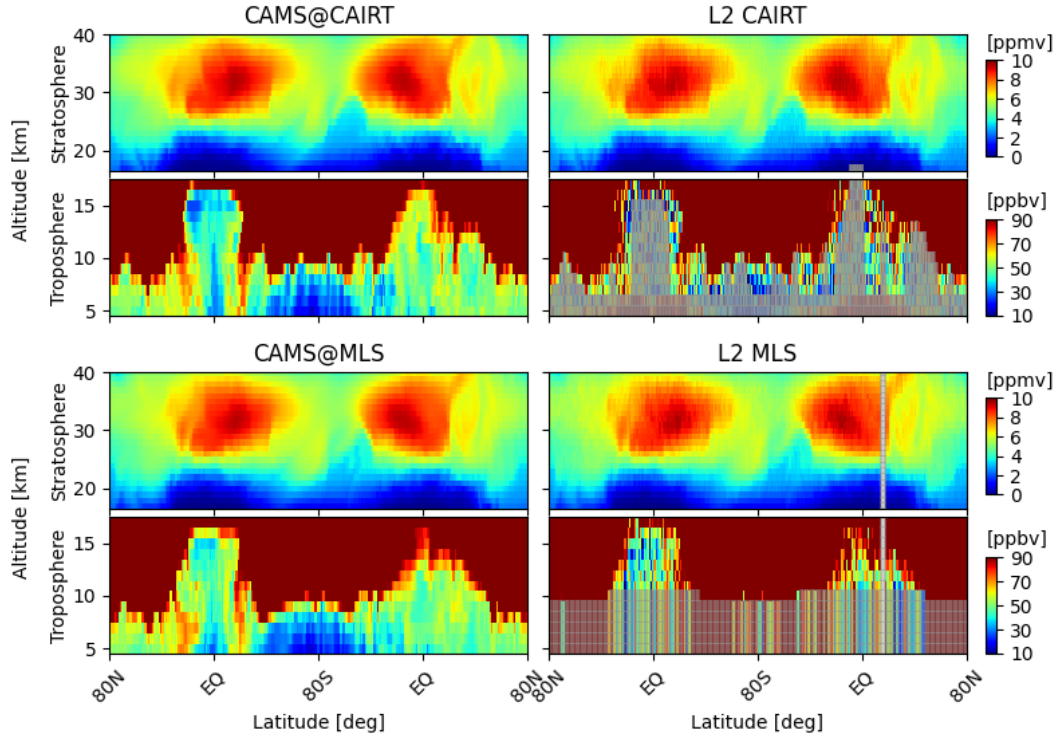

Figure 5. (top panels) Ozone along the first complete CAIRT orbit on Dec. 15, 2021 for track 2. The left panel shows the CAMS nature run interpolated on the CAIRT orbit, while the right panel shows the CAIRT simulated L2 observations. The top panel is split into two parts for the stratosphere portion (top, in ppmv) and the troposphere (bottom, in ppbv). Gray areas denote observations obscured by clouds or rejected below 7 km due to a too-large systematic error. (bottom panels) As top for MLS for the closest orbit to CAIRT on the same date. Here, invalid MLS data are indicated by the gray area.

Six BASCOE experiments were performed, as summarized in Table 2. The first is a control run (CR) without data assimilation. The second is an assimilation run using simulated MLS profiles (AR_{MLS}). Two additional assimilation runs were conducted with simulated CAIRT superobservation profiles: the first assumes a 400 km swath (AR_{CAIRT}), which corresponds to the default configuration adopted during the CAIRT Phase A study, and the second assumes a 300 km swath (AR_{C300km}), representing the threshold value for CAIRT. Since the simulated MLS profiles do not include any systematic error, an additional assimilation run was performed using CAIRT superobservations excluding the contribution of systematic error (AR_{Cnosys}). Finally, to assess the potential impact of clouds, a sixth assimilation run ($AR_{Cnocloud}$) was carried out using the simulated CAIRT superobservation profiles with a 400 km swath, excluding the contribution of systematic error and without cloud filtering.

The control run was initialized from the nature run on 15 August 2021, whereas all assimilation runs were initialized on 15 September 2021 from the control run. All simulations are evaluated against the nature run for the period from October 2021 to February 2022, allowing for a 15-day spin-up period for each assimilation experiment.

https://doi.org/10.5194/egusphere-2025-6130
Preprint. Discussion started: 27 December 2025

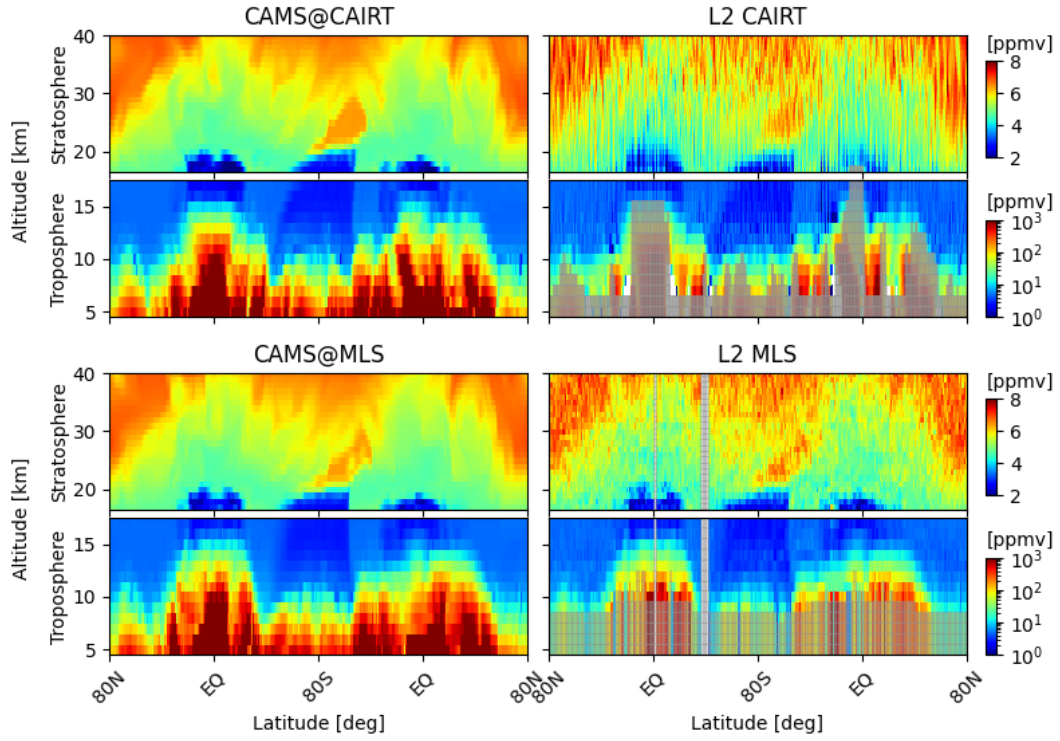

Figure 6. As Fig. 4 but for water vapour. Note the logarithmic color bar in the troposphere.

Table 2. Summary of model simulations and data assimilation experiments used in this study.

Label	Model	Model resolution (nlat×nlon×nlev)	Assimilated observations
NR	IFS-COMPO 47r3	512×1024×137	Meteorological observations
CR	BASCOE-CTM	91×144×51	None
AR_{MLS}	BASCOE-EnKF	91×144×51	Simulated MLS L2 profiles
AR_{CAIRT}	BASCOE-EnKF	91×144×51	Simulated CAIRT L2 superobservation profiles based on CAIRT L2 400 km swath
AR_{C300km}	BASCOE-EnKF	91×144×51	As in AR_{CAIRT} but based on CAIRT L2 300 km swath
AR_{Cnosys}	BASCOE-EnKF	91×144×51	As in AR_{CAIRT} without systematic error
$AR_{Cnocloud}$	BASCOE-EnKF	91×144×51	As in AR_{Cnosys} without cloud filtering

https://doi.org/10.5194/egusphere-2025-6130
Preprint. Discussion started: 27 December 2025

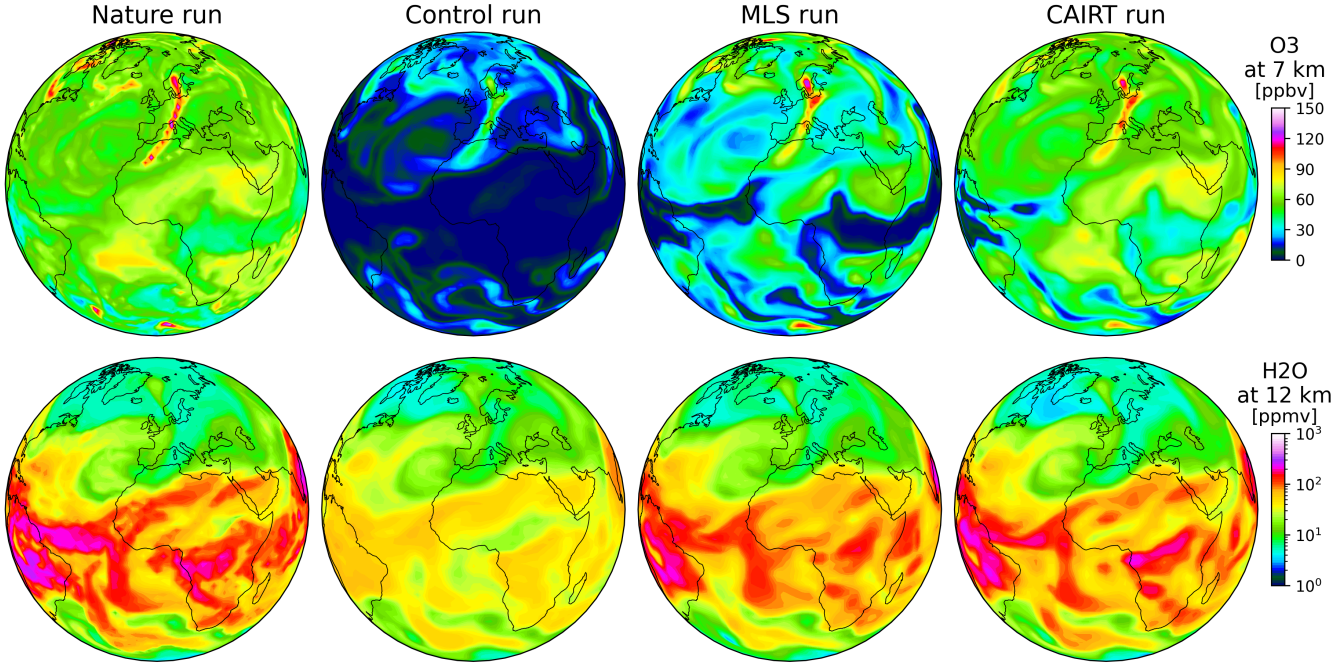

Figure 7. (top) Ozone distribution [ppbv] at 7 km of altitude on Dec. 3, 2021 at 0 UT for (from left to right) the reference nature run, the control run, the MLS assimilation run and the CAIRT assimilation run. (bottom) As top but for H2O at 12 km of altitude.

8 Results

CAIRT data help to improve the representation of ozone and water vapour, as illustrated in Fig. 7. The ozone distribution is shown at 7 km during a tropopause fold event above Europe, which is well represented by both the CAIRT and MLS assimilation runs, effectively correcting the bias present in the control run. One can also see the strong constraint provided by CAIRT observations, which substantially—though not completely—reduces the negative bias of the control run outside the tropopause fold region, and to a greater extent than MLS data. Similarly, CAIRT observations also provide a significant constraint, comparable to that of MLS, in the representation of water vapour at 12 km.

8.1 Ozone

Figure 8 shows the statistical differences between the nature run and the various BASCOE runs for the period October 2021–February 2022 (five months), as a function of latitude and altitude for ozone. The statistics displayed are the normalized mean bias (NMB), the normalized standard deviation (NSD), and the correlation coefficient. Before computing these statistics, the nature run was downgraded to the spatial resolution of the BASCOE runs.

As shown in Fig. 8, there are large differences between the control and nature runs: the BASCOE ozone chemistry predicts lower ozone concentrations in the stratosphere and higher ozone in the troposphere. Assimilating MLS data enables the BAS-

https://doi.org/10.5194/egusphere-2025-6130
Preprint. Discussion started: 27 December 2025

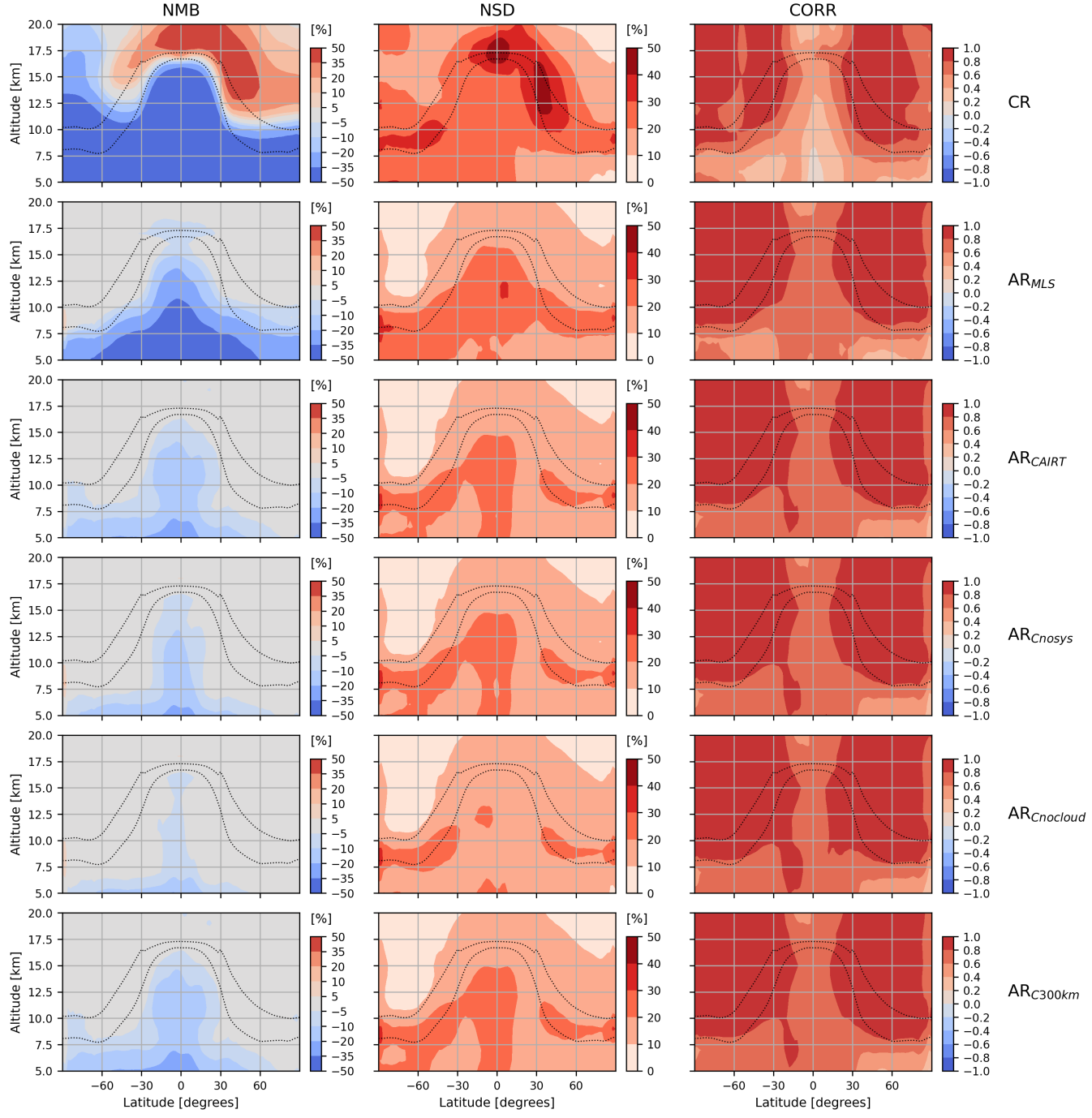

Figure 8. (Left column) Ozone zonal mean normalized mean bias (NMB, in %) between the nature run (NR) and, from top to bottom, the control run (CR), the MLS assimilation run (MLS) and the CAIRT assimilation run for the period October 2021 – February 2022. (Middle column) The associated normalized standard deviation (NSD, in %) of the differences shown in top line. (Right column) The correlation between the runs shown in top line.

https://doi.org/10.5194/egusphere-2025-6130
Preprint. Discussion started: 27 December 2025

COE system to largely remove the ozone bias in the stratosphere and the tropopause region, accompanied by a strong reduction in the standard deviation and a significant increase in correlation compared to the control run. In the troposphere, while a large part of the control run bias is eliminated and the correlation with the nature run increases, a residual bias of about –45 % remains in the tropics around 7.5 km altitude.

The situation improves markedly when CAIRT observations are assimilated. The bias in the tropics around 7.5 km decreases to values between –15 % and –25 %, representing a clear improvement compared to MLS. The standard deviation of the differences and the correlation coefficients are also improved when assimilating CAIRT rather than MLS data.

Since the simulation of MLS data does not include systematic error, an additional assimilation run using CAIRT data without systematic error was performed to ensure a fair comparison between both instruments. This configuration shows a substantial improvement in the bias in the tropical tropopause compared to AR_{CAIRT}, with the remaining bias mainly attributable to data scarcity and random error. When the cloud mask is disabled – thus including all profiles, even those excluded by clouds – and excluding the systematic error, the bias further decreases to between –5 % and –10 %, as shown by experiment $AR_{Cnocloud}$. Finally, reducing the swath width to 300 km does not significantly affect CAIRT's capability to observe ozone in the UTLS (see experiment AR_{C300km} in Fig. 8).

These results confirm the capability of CAIRT to provide valuable ozone information from the stratosphere down to about 7 km in the upper troposphere.

8.2 Water vapour

Figure 9 shows the statistical differences between the nature run and the other BASCOE runs, this time for water vapour. As before, large discrepancies are observed between NR and CR. The improvements due to data assimilation are comparable in the stratosphere for all assimilated datasets: the bias is almost completely eliminated, and the correlation is substantially enhanced. AR_{MLS} displays slightly better performance than AR_{CAIRT} around the tropopause, while AR_{CAIRT} provides marginally lower bias and standard deviation in the troposphere. The results of experiments $AR_{Cnocloud}$ and AR_{Cnosys} indicate that the negative bias between 10 and 15 km is due to the presence of clouds and to the systematic error of CAIRT. As for ozone, reducing the CAIRT swath to 300 km does not noticeably reduce the constraint of CAIRT on the BASCOE system.

Compared to ozone, the constraint of CAIRT water vapour observations on the BASCOE system is considerably weaker in the troposphere. This is likely due to the limited representation of water vapour physical processes in BASCOE. The condensation scheme implemented in BASCOE successfully produces a dry tropopause but removes too much water vapour in the mid-troposphere, resulting in a dry bias across all BASCOE experiments. Nevertheless, the primary objective of CAIRT water vapour profiles is to reduce the temperature bias in the UTLS in NWP systems, thereby improving forecast quality. In the troposphere, NWP systems already benefit from humidity observations provided by nadir-viewing satellite instruments and radiosondes.

https://doi.org/10.5194/egusphere-2025-6130
Preprint. Discussion started: 27 December 2025

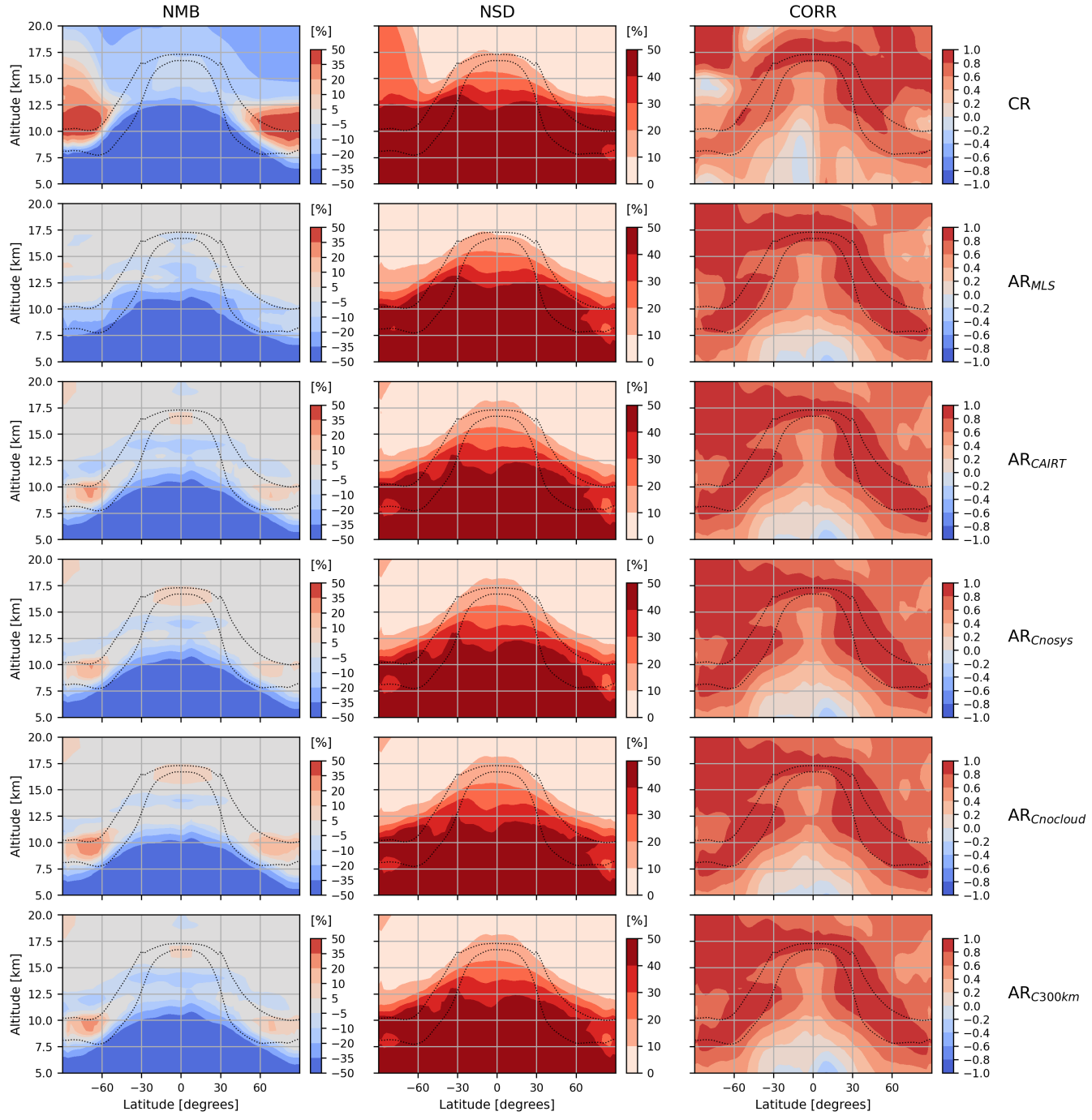

Figure 9. As Fig. 8 but for water vapour.

https://doi.org/10.5194/egusphere-2025-6130
Preprint. Discussion started: 27 December 2025

9 Conclusions

This study evaluated the added value of ozone and water vapour profiles from the proposed satellite limb instrument CAIRT, designed to observe the temperature and composition of the middle atmosphere. The evaluation was conducted through an Observing System Simulation Experiment (OSSE) using an IFS model simulation as the nature run and the BASCOE system to perform the control and assimilation runs. CAIRT observations were simulated through a comprehensive processing chain starting from the IFS model fields as the synthetic truth, and accounting for CAIRT's orbit, geographical coverage, cloud contamination, spatial and spectral resolution, error budget, and super-observation strategy. For comparison, MLS profiles of ozone and water vapour were also simulated from the same IFS synthetic truth and assimilated by BASCOE, to assess the relative added value of CAIRT against an existing limb sounder.

For ozone, the OSSE results show that CAIRT can provide valuable information down to the mid-troposphere. Compared with the nature run, the BASCOE control run exhibits a positive bias above the tropopause and a negative bias in the troposphere exceeding ± 50 %. Assimilating either MLS or CAIRT observations reduces the bias to within ± 5 % above the tropopause. In the tropopause region, CAIRT performs slightly better than MLS, with biases below ± 5 %, whereas MLS data cannot fully remove a residual bias between -10 % and -5 % in the tropics. In the troposphere, MLS assimilation significantly reduces the control run bias, but a notable residual remains (-5 % at high latitudes to more than -35 % in the tropical lower troposphere). CAIRT data provide a stronger constraint, reducing the bias to below -5 % in the extra-tropics and below -20 % in the tropics. Additional runs indicate that the remaining bias in the tropical troposphere is due to the presence of cloud and to CAIRT's systematic error. Furthermore, reducing the CAIRT swath from 400 km to 300 km has little impact, suggesting that a narrower swath could be implemented if required by technical constraints without significant loss of performance.

For water vapour, CAIRT can provide useful information down to about 10 km in the extra-tropics and 15 km in the tropics, with a constraint comparable to that of MLS. As for O_3, reducing the swath to 300 km does not significantly affect CAIRT's ability to constrain the UTLS. Overall, these results indicate that CAIRT could deliver high-quality water vapour profiles suitable for constraining the UTLS region providing invaluable data to improve numerical weather prediction (NWP) systems.

CAIRT would provide invaluable data to improve weather forecasting

This OSSE therefore demonstrates that CAIRT data are capable of meeting the mission's scientific objectives in the UTLS, particularly by improving the characterization of vertical gradients and small-scale structures of ozone and water vapour across the tropopause. Such capabilities directly support CAIRT's overarching goal of advancing our understanding of the coupling between atmospheric composition, circulation, and climate.

Code and data availability. CAMS control simulation can be retrieved from the ECMWF MARS archiving system using the following parameters: class=rd, stream=oper, expver=hlqd, type=fc, time=00:00:00, step=3/6/9/12/15/18/21/24, levtype=ml, levelist=all, param=z/t/q/o3/cc/lnsp, grid=F256.

CAIRT orbit file is available here: https://doi.org/10.5281/zenodo.10262729.

https://doi.org/10.5194/egusphere-2025-6130
Preprint. Discussion started: 27 December 2025

Simulating the CAIRT L2 grid is done using CAIRT orbit file and the the CAIRT grid simulator python code sim_CAIRT_grid.py v1.0.0 maintained at the Jülich git repository (https://jugit.fz-juelich.de/cairt-scirec/sim_CAIRT_grid).

The CAMS interpolated product on the CAIRT grid are archived at BIRA-IASB and can be obtained by emailing to quentin.errera@aeronomie.be.

The simulated CAIRT L2 observations of ozone and water vapour are archived at BIRA-IASB and can be obtained by emailing to quentin.errera@aeronomie.be. They are simulated using the CAMS interpolated product on the CAIRT grid files and the CAIRT L2 simulator.This code and its configuration files are maintained at the Jülich github repository (https://jugit.fz-juelich.de/cairt-scirec/cairt_fl2s).

MLS v5 daily observation files can be downloaded here: https://mls.jpl.nasa.gov/eos-aura-mls/data.php.

BASCOE outputs may be available by emailing to quentin.errera@aeronomie.be.

Author contributions. QE conducted the study: downloading the CAMS data, producing the simulations of CAIRT and MLS data, running the BASCOE experiments, generating the figures, coordinating the writing of the manuscript, and writing most sections. BMS and AH contributed to Sects. 1 and 2. JF supported QE in writing Sect. 3. GP simulated the CAIRT orbit and wrote Sect. 4.1. JU and DP contributed to the code used to simulate the CAIRT L2 grid and to writing Sect. 4.2. MH performed the spectra/Jacobian calculations, developed the instrument simulator and contributed to the writing of Sect. 4.4. BF, with the support of SF, developed the L2 performance estimation and profile-simulation algorithms and generated the L2 performance files. BF contributed to the writing of Sect. 4.5. PR developed the cloud-masking code and contributed to the writing of Sect. 4.5. NL supported QE in the simulation of MLS data. MO supported QE in the analysis of the results. All authors reviewed the full manuscript and approved it prior to submission.

Competing interests. At least one of the (co-)authors is a member of the editorial board of Atmospheric Measurement Techniques.

Acknowledgements. This work was supported by ESA via the CAIRT Performance and Requirement Consolidation study (PerReC) under the ESA/ESTEC contract 4000136480/21/NL/LF CCN1. Work at the Jet Propulsion Laboratory, California Institute of Technology, was performed under contract with the National Aeronautics and Space Administration (80NM0018D0004). The text of this manuscript has been revised by ChatGPT before the final reading by the authors.

https://doi.org/10.5194/egusphere-2025-6130
Preprint. Discussion started: 27 December 2025

References

Abalos, M., Orbe, C., Kinnison, D. E., Plummer, D., Oman, L. D., Jöckel, P., Morgenstern, O., Garcia, R. R., Zeng, G., Stone, K. A., and Dameris, M.: Future trends in stratosphere-to-troposphere transport in CCMI models, Atmos. Chem. Phys., 20, 6883–6901, https://doi.org/doi.org/10.5194/acp-20-6883-2020, 2020.

Abida, R., Attié, J.-L., El Amraoui, L., Ricaud, P., Lahoz, W., Eskes, H., Segers, A., Curier, L., de Haan, J., Kujanpää, J., Nijhuis, A. O., Tamminen, J., Timmermans, R., and Veefkind, P.: Impact of spaceborne carbon monoxide observations from the S-5P platform on tropospheric composition analyses and forecasts, Atmos. Chem. Phys., 17, 1081–1103, https://doi.org/10.5194/acp-17-1081-2017, 2017.

Arola, A., Basart, S., Benedictow, A., Bennouna, Y., Blechschmidt, A.-M., Bouarar, I., Cuevas, E., Errera, Q., Eskes, H., Griesfeller, J., Kapsomenakis, J., Langerock, B., Mortier, A., Pison, I., Pitkänen, M., Ramonet, M., Richter, A., Schulz, M., Tarniewicz, J., Thouret, V., Tsikerdekis, A., Warneke, T., and Zerefos, C.: Validation report of the CAMS near-real-time global atmospheric composition service: December 2021 – February 2022, Copernicus atmosphere monitoring service (CAMS) report, https://doi.org/10.24380/9z4h-5niy, cAMS2_82 o-suite quarterly report, 2022.

Bland, J., Gray, S., Methven, J., and Forbes, R.: Characterising extratropical near-tropopause analysis humidity biases and their radiative effects on temperature forecasts, Q. J. R. Meteorol. Soc., 147, 3878–3898, https://doi.org/https://doi.org/10.1002/qj.4150, 2021.

Butchart, N.: The Brewer-Dobson circulation, Rev. Geophys., 52, 157–184, https://doi.org/https://doi.org/10.1002/2013RG000448, 2014.

Charlesworth, E., Plöger, F., Birner, T., Baikhadzhaev, R., Abalos, M., Abraham, N. L., Akiyoshi, H., Bekki, S., Dennison, F., Jöckel, P., Keeble, J., Kinnison, D., Morgenstern, O., Plummer, D., Rozanov, E., Strode, S., Zeng, G., Egorova, T., and Riese, M.: Stratospheric water vapor affecting atmospheric circulation, Nat. Commun., 14, 3925, https://doi.org/10.1038/s41467-023-39559-2, number: 1 Publisher: Nature Publishing Group, 2023.

Claeyman, M., Attié, J.-L., Peuch, V.-H., El Amraoui, L., Lahoz, W. A., Josse, B., Joly, M., Barré, J., Ricaud, P., Massart, S., Piacentini, A., von Clarmann, T., Höpfner, M., Orphal, J., Flaud, J.-M., and Edwards, D. P.: A thermal infrared instrument onboard a geostationary platform for CO and O_3 measurements in the lowermost troposphere: Observing System Simulation Experiments (OSSE), Atmos. Meas. Tech., 4, 1637–1661, https://doi.org/10.5194/amt-4-1637-2011, 2011.

Duncan, D. I., Bormann, N., Geer, A. J., and Weston, P.: Superobbing and Thinning Scales for All-Sky Humidity Sounder Assimilation, Mon. Weather Rev., 152, 1821 – 1837, https://doi.org/10.1175/MWR-D-24-0020.1, 2024.

Errera, Q., Funke, B., Hoffmann, A., Höpfner, M., Raspollini, P., Sinnhuber, B.-M., Walker, and K.: Extended Reference Scenarios (ERS) for the ESA Earth Explorer 11 candidate CAIRT (Changing Atmosphere Infra-Red Tomography explorer), Earth Syst. Sci. Data, in prep.

Errera, Q., Dekemper, E., Baker, N., Debosscher, J., Demoulin, P., Mateshvili, N., Pieroux, D., Vanhellemont, F., and Fussen, D.: On the capability of the future ALTIUS ultraviolet–visible–near-infrared limb sounder to constrain modelled stratospheric ozone, Atmos. Meas. Tech., 14, 4737–4753, https://doi.org/doi.org/10.5194/amt-14-4737-2021, 2021.

ESA: Earth Observation Mission Software File Format Specification, Reference: PE-ID-ESA-GS-584, Issue: 1, Revision: 9, https://eop-cfi.esa.int/Repo/PUBLIC/DOCUMENTATION/SYSTEM_SUPPORT_DOCS/PE-ID-ESA-GS-584-EO_Mission_SW_File_Format_Specs_latest.pdf, 2024.

ESA: Report for Mission Selection: Earth Explorer 11 Candidate Mission CAIRT, European Space Agency, Noordwijk, The Netherlands, ESA-EOPSM-CAIR-RP-4797, 230 pp., https://doi.org/10.5281/zenodo.15606819, 2025a.

ESA: ESA Mission CFI Software, https://eop-cfi.esa.int/index.php/mission-cfi-software/eocfi-software, 2025b.

https://doi.org/10.5194/egusphere-2025-6130
Preprint. Discussion started: 27 December 2025

ESA: Earth Observation Mission CFI Software, Quick Start Guide, Code EO-MA-DMS-GS-0009, Issue: 4.29, https://eop-cfi.esa.int/index.php/mission-cfi-software/eocfi-software/branch-4-x/eocfi-v4x-documentation, 2025c.

Eskes, H. J., van Velthoven, P. F. J., Valks, P. J. M., and Kelder, H. M.: Assimilation of GOME total-ozone satellite observations in a three-dimensional tracer-transport model, Q. J. R. Meteorol. Soc., 129, 1663–1681, https://doi.org/10.1256/qj.02.14, 2003.

Fischer, H., Birk, M., Blom, C., Carli, B., Carlotti, M., von Clarmann, T., Delbouille, L., Dudhia, A., Ehhalt, D., Endemann, M., Flaud, J. M., Gessner, R., Kleinert, A., Koopmann, R., Langen, J., López-Puertas, M., Mosner, P., Nett, H., Oelhaf, H., Perron, G., Remedios, J., Ridolfi, M., Stiller, G., and Zander, R.: MIPAS: an instrument for atmospheric and climate research, Atmos. Chem. Phys., 8, 2151–2188, https://doi.org/10.5194/acp-8-2151-2008, 2008.

Flemming, J., Huijnen, V., Arteta, J., Bechtold, P., Beljaars, A., Blechschmidt, A.-M., Diamantakis, M., Engelen, R. J., Gaudel, A., Inness, A., Jones, L., Josse, B., Katragkou, E., Marecal, V., Peuch, V.-H., Richter, A., Schultz, M. G., Stein, O., and Tsikerdekis, A.: Tropospheric chemistry in the Integrated Forecasting System of ECMWF, Geosci. Model Dev., 8, 975–1003, https://doi.org/10.5194/gmd-8-975-2015, 2015.

Forbes, R., Laloyaux, P., and Rodwell, M.: IFS upgrade improves moist physics and use of satellite observations, ECMWF Newsletter, 169, 17–24, https://www.ecmwf.int/sites/default/files/elibrary/102021/20225-newsletter-no-169-autumn-2021_1.pdf, 2021.

Friedl-Vallon, F., Gulde, T., Hase, F., Kleinert, A., Kulessa, T., Maucher, G., Neubert, T., Olschewski, F., Piesch, C., Preusse, P., Rongen, H., Sartorius, C., Schneider, H., Schönfeld, A., Tan, V., Bayer, N., Blank, J., Dapp, R., Ebersoldt, A., Fischer, H., Graf, F., Guggenmoser, T., Höpfner, M., Kaufmann, M., Kretschmer, E., Latzko, T., Nordmeyer, H., Oelhaf, H., Orphal, J., Riese, M., Schardt, G., Schillings, J., Sha, M. K., Suminska-Ebersoldt, O., and Ungermann, J.: Instrument concept of the imaging Fourier transform spectrometer GLORIA, Atmos. Meas. Tech., 7, 3565–3577, https://doi.org/10.5194/amt-7-3565-2014, 2014.

Funke, B., Höpfner, M., Bender, S., Errera, Q., Hoffmann, A., Raspollini, P., Sinnhuber, B.-M., and Ungermann., J.: Linear tomographic performance estimation for the Changing Atmosphere Infra-Red Tomography explorer (CAIRT) mission concept, Atmos. Meas. Tech., in prep.

Gettelman, A., Mills, M. J., Kinnison, D. E., Garcia, R. R., Smith, A. K., Marsh, D. R., Tilmes, S., Vitt, F., Bardeen, C. G., McInerny, J., Liu, H.-L., Solomon, S. C., Polvani, L. M., Emmons, L. K., Lamarque, J.-F., Richter, J. H., Glanville, A. S., Bacmeister, J. T., Phillips, A. S., Neale, R. B., Simpson, I. R., DuVivier, A. K., Hodzic, A., and Randel, W. J.: The Whole Atmosphere Community Climate Model Version 6 (WACCM6), J. Geophys. Res., 124, 12 380–12 403, https://doi.org/https://doi.org/10.1029/2019JD030943, 2019.

Hegglin, M. I. and Shepherd, T. G.: Large climate-induced changes in ultraviolet index and stratosphere-to-troposphere ozone flux, Nat. Geosci., 2, https://doi.org/doi:10.1038/NGEO604, 2009.

Hoffman, R. N.: The Effect of Thinning and Superobservations in a Simple One-Dimensional Data Analysis with Mischaracterized Error, Mon. Weather Rev., 146, 1181 – 1195, https://doi.org/10.1175/MWR-D-17-0363.1, 2018.

Hsu, J. and Prather, M. J.: Stratospheric variability and tropospheric ozone, J. Geophys. Res., 114, https://doi.org/https://doi.org/10.1029/2008JD010942, 2009.

Lacis, A. A., Wuebbles, D. J., and Logan, J. A.: Radiative forcing of climate by changes in the vertical distribution of ozone, J. Geophys. Res., 95, 9971–9981, https://doi.org/https://doi.org/10.1029/JD095iD07p09971, 1990.

Li, F., Waugh, D. W., Douglass, A. R., Newman, P. A., Strahan, S. E., Ma, J., Nielsen, J. E., and Liang, Q.: Long-term changes in stratospheric age spectra in the 21st century in the Goddard Earth Observing System Chemistry-Climate Model (GEOSCCM), J. Geophys. Res., 117, https://doi.org/https://doi.org/10.1029/2012JD017905, 2012.

https://doi.org/10.5194/egusphere-2025-6130
Preprint. Discussion started: 27 December 2025

Livesey, N. J., Read, W. G., Wagner, P. A., Froidevaux, L., Santee, M., Schwartz, M. J., Lambert, A., Millán Valle, L. F., Pumphrey, H. C., Manney, G. L., Fuller, R. A., Jarnot, R. F., Knosp, B. W., and Lay, R. R.: Earth Observing System (EOS) Aura Microwave Limb Sounder (MLS) Version 5.0x Level 2 and 3 data quality and description document, Tech. Rep. D-105336 Rev. B, JPL, https://mls.jpl.nasa.gov/data/v5-0_data_quality_document.pdf, 2022.

Masutani, M., Schlatter, T. W., Errico, R. M., Stoffelen, A., Andersson, E., Lahoz, W., Woollen, J. S., Emmitt, G. D., Riishøjgaard, L.-P., and Lord, S. J.: Observing System Simulation Experiments, in: Data Assimilation, edited by Lahoz, William, Khattatov, Boris, Menard, and Richard, pp. 647–679, Springer Berlin Heidelberg, ISBN 978-3-540-74702-4, https://doi.org/10.1007/978-3-540-74703-1_24, 2010.

McLandress, C. and Shepherd, T. G.: Simulated Anthropogenic Changes in the Brewer–Dobson Circulation, Including Its Extension to High Latitudes, J. Climate, 22, 1516 – 1540, https://doi.org/10.1175/2008JCLI2679.1, 2009.

Millán, L., Santee, M. L., Lambert, A., Livesey, N. J., Werner, F., Schwartz, M. J., Pumphrey, H. C., Manney, G. L., Wang, Y., Su, H., Wu, L., Read, W. G., and Froidevaux, L.: The Hunga Tonga-Hunga Ha'apai Hydration of the Stratosphere, Geophys. Res. Lett., 49, e2022GL099 381, https://doi.org/https://doi.org/10.1029/2022GL099381, 2022.

Murphy, D. M. and Koop, T.: Review of the vapour pressures of ice and supercooled water for atmospheric applications, Quarterly Journal of the Royal Meteorological Society, 131, 1539–1565, https://doi.org/10.1256/qj.04.94, 2005.

Norton, R. H. and Beer, R.: New apodizing functions for Fourier spectrometry, J. Opt. Soc. Am., 66, 259–264, https://doi.org/10.1364/JOSA.66.000259, 1976.

Norton, R. H. and Beer, R.: Errata: New Apodizing Functions For Fourier Spectrometry, J. Opt. Soc. Am., 67, 419–419, https://doi.org/10.1364/JOSA.67.000419, 1977.

Riese, M., Ploeger, F., Rap, A., Vogel, B., Konopka, P., Dameris, M., and Forster, P.: Impact of uncertainties in atmospheric mixing on simulated UTLS composition and related radiative effects, J. Geophys. Res., 117, https://doi.org/https://doi.org/10.1029/2012JD017751, 2012.

Riese, M., Oelhaf, H., Preusse, P., Blank, J., Ern, M., Friedl-Vallon, F., Fischer, H., Guggenmoser, T., Höpfner, M., Hoor, P., Kaufmann, M., Orphal, J., Plöger, F., Spang, R., Suminska-Ebersoldt, O., Ungermann, J., Vogel, B., and Woiwode, W.: Gimballed Limb Observer for Radiance Imaging of the Atmosphere (GLORIA) scientific objectives, Atmos. Meas. Tech., 7, 1915–1928, https://doi.org/10.5194/amt-7-1915-2014, 2014.

Rijsdijk, P., Eskes, H., Dingemans, A., Boersma, K. F., Sekiya, T., Miyazaki, K., and Houweling, S.: Quantifying uncertainties in satellite NO_2 superobservations for data assimilation and model evaluation, Geosci. Model Dev., 18, 483–509, https://doi.org/10.5194/gmd-18-483-2025, 2025.

Semane, N. and Bonavita, M.: Reintroducing the analysis of humidity in the stratosphere, https://doi.org/doi.org/10.21957/ns41h80kl3, 2025.

Sinnhuber, B.-M., Chipperfield, M. P., Dinelli, B. M., Errera, Q., Friedl-Vallon, F., Funke, B., Godin-Beekmann, S., Hoffmann, A., Holm, E., Höpfner, M., Malavart, A., Monge-Sanz, B. M., Op de beeck, M., Osprey, S., Papandrea, E., Polichtchouk, I., Preusse, P., Raspollini, P., Rhode, S., Riese, M., Sellitto, P., Ungermann, J., Vervalcke, S., Verronen, P., Voet, F., and Walker, K. A.: The Changing-Atmosphere Infrared Tomography Explorer CAIRT – an infrared limb-imaging satellite concept to chart the middle atmosphere in the climate system, Bull. Amer. Meteor. Soc., in reveiw.

Solomon, S., Rosenlof, K. H., Portmann, R. W., Daniel, J. S., Davis, S. M., Sanford, T. J., and Plattner, G.-K.: Contributions of Stratospheric Water Vapor to Decadal Changes in the Rate of Global Warming, Science, 327, 1219–1223, https://doi.org/10.1126/science.1182488, 2010.

https://doi.org/10.5194/egusphere-2025-6130
Preprint. Discussion started: 27 December 2025

SPARC: The SPARC Data Initiative: Assessment of stratospheric trace gas and aerosol climatologies from satellite limb sounders, M. I. Hegglin and S. Tegtmeier (Eds.) and SPARC Report No. 8, https://doi.org/10.3929/ethz-a-010863911, 2017.

Steck, T., Höpfner, M., von Clarmann, T., and Grabowski, U.: Tomographic retrieval of atmospheric parameters from infrared limb emission observations, Appl. Opt., 44, 3291–3301, https://doi.org/10.1364/AO.44.003291, 2005.

Stiller, G.: The Karlsruhe Optimized and Precise Radiative transfer Algorithm (KOPRA), Tech. rep., Froschungszentrum Karlsruhe, https://doi.org/10.5445/IR/270048971, 2000.

Timmermans, R., Lahoz, W., Attié, J.-L., Peuch, V.-H., Curier, R., Edwards, D., Eskes, H., and Builtjes, P.: Observing System Simulation Experiments for air quality, Atmos. Environ., 115, 199 – 213, https://doi.org/https://doi.org/10.1016/j.atmosenv.2015.05.032, 2015.